Probing the origins and control of shrinkage stress in dental resin-composites: I. Shrinkage stress characterization technique*

H. LU[1], J. W. STANSBURY[1,2], S. H. DICKENS[3], F. C. EICHMILLER[3], C. N. BOWMAN[1,2]†
[1]*Department of Chemical and Biological Engineering, University of Colorado, Boulder, CO 80309, USA*
E-mail: Christopher.Bowman@colorado.edu
[2]*Department of Restorative Dentistry, University of Colorado Health Sciences Center, Denver, CO 80262, USA*
[3]*American Dental Association Foundation, Paffenbarger Research Center, Gaithersburg, MD 20899, USA*

The accurate and reliable characterization of the polymerization shrinkage stress is becoming increasingly important, as the shrinkage stress still is a major drawback of current dimethacrylate-based dental materials and restricts its range of applications. The purpose of this research is to develop a novel shrinkage stress measurement device to elucidate the shrinkage stress evolution of dental restorative composites while allowing for controlled sample deformation during the polymerization. Furthermore, the device is designed to mimic the clinically relevant cusp-to-cusp displacement by systematically adjusting the instrument compliance, the bonded surface area/unbonded area by sample geometry, and the total bonded area by sample diameter. The stress measurement device based on the cantilever beam deflection theory has been successfully developed and characterized using a commercial dental composite. It was shown that this device is a highly effective, practical and reliable shrinkage stress measurement tool, which enables its facile applications to the investigation of shrinkage stress kinetics of both commercial and experimental composites, as well as for probing various aspects that dictate shrinkage stress development.

1. Introduction

Over the last 40 years, dimethacrylate based dental resins have become widely utilized in restorative dentistry. However, volumetric shrinkage and shrinkage stress arising during polymerization still remain as the foremost shortcomings of current dental resin systems [1, 2]. Shrinkage stress transferred to the tooth may lead to the deformation of the cusp or even enamel microcracks [2–4], while shrinkage stresses at the tooth-composite interface have the potential to cause adhesive failure, initiating microleakage and recurrent caries. As the magnitude and distribution of the polymerization shrinkage stress have a dramatic impact on the performance and longevity of the restorations, the investigation of the shrinkage stress during the polymerization of dental restorative composites has received worldwide attention since the 1960s [5–8].

While shrinkage stress associated with dental resin composites has been investigated for several decades, the techniques employed to characterize the stress development are very limited. The techniques that researchers have used include the photoelastic method [9, 10], stress–strain-analyzer testing machine [11] and finite element analysis [12, 13]. However, the mostly widely used shrinkage stress characterization tool is based on the universal testing machine (UTM) and frequently referred to as a tensilometer [14–18], where the sample assembly was mounted vertically between the crosshead and a tensile load cell of the UTM. The distance between the crosshead and tensile load cell was kept constant while the load cell recorded the tensile force required to counteract the sample deformation as the sample polymerized and contracted. The shrinkage stress was then obtained by dividing the

*Certain commercial materials and equipment are identified in this paper for adequate definition of the experimental procedure. In no instance does such identification imply recommendation or endorsement by the National Institute of Standards and Technology or the ADA Foundation or that the material or equipment identified is necessarily the best available for the purpose.
†Author to whom all correspondence should be addressed.

measured tensile force by the cross-sectional area of the sample.

Despite its popularity, there are also several considerable limitations of using the UTM-based tensilometer technique. First, constant strain is maintained through a servo-controlled recovery system; no sample deformation was allowed to occur despite the large shrinkage stress. In contrast, in the clinical practice the natural teeth and oral tissue complex have only limited rigidity, which implies that it is capable of deforming to a certain degree under the shrinkage stress during polymerizations. This observation is also supported by measurements of the cusp-to-cusp deflection ranging from 10 to 30 μm during composite polymerization [3, 4, 19, 20]. Second, since an external feedback load needs to be applied to maintain a constant sample height, the sample was constantly being contracted under the shrinkage and stretched by the corresponding feedback force. This pseudo-cycling behavior during the shrinkage stress measurement is inevitably affected by the instrument feedback parameter settings and the dynamics of sample modulus development.

Recently, Watts *et al*. has reported a newly-developed shrinkage stress measurement device that is based on the cantilever load cell [21]. The uni-axial shrinkage stresses of four different commercial light-cured dental composites have been investigated. Very good reproducibility has been achieved using this device. However, the device and methodology also contain several limitations: (1) the cantilever system is a fixed compliance system; (2) the disk-shape sample (10 mm in diameter with 0.8 mm and 1.2 mm thickness) has an average aspect ratio of 10, which is much higher than the aspect ratio of the cavities encountered in clinical situation. In addition, as investigated by Laughlin *et al*., the higher the aspect ratio, the more error of assuming uni-axial shrinkage stress distribution [13]. (3) Re-normalization of the stress-data was implemented by multiplying a correction factor of four on the raw-stress values.

Therefore, an experimental approach to measure the shrinkage stress, capable of imitating the clinical situation with known deformation mimicking that of the opposing cusps would be valuable to develop. As discussed above, natural teeth are deformable to a certain extent and relieve part of the shrinkage stress that would otherwise be generated within the oral tissues. Although it is impossible to perfectly mimic the exact modulus and deformation limit of different teeth with various cavity configurations, a shrinkage stress measurement device with variable compliance is especially valuable in the investigation of the shrinkage stress development. The purpose of this research is to develop a novel shrinkage stress device that is capable of measuring the shrinkage stress of composites or resins while allowing for controlled sample deformation and sample geometry during the polymerization. The device is designed to mimic the clinically relevant cusp-to-cusp displacement by adjusting the instrument compliance and the filling geometry by varying the sample diameter and length. The ultimate goal is to develop a practical and accurate benchtop shrinkage stress device that could measure the ultimate shrinkage stress value as well as probe the kinetics of stress evolution for both composite and neat resin systems.

2. Materials and methods

2.1. Methods

The shrinkage stress device, referred to hereafter as a tensometer, and the corresponding software program were fabricated and designed at the Paffenbarger Research Center (PRC) of the American Dental Association Foundation (ADAF), located at the National Institute of Standards and Technology (NIST). This device is based on the basic engineering beam theory that a tensile force generated by the bonded shrinking sample (composite or resin) causes a cantilever beam to deflect. The deflection of the beam is measured with a linear variable differential transformer (LVDT). The tensile force is calculated based upon a previously obtained calibration constant for the beam, and this calibration constant is dependent on the distance between the clamped end of the cantilever beam and the sample position along the beam (Beam Length). The shrinkage stress was obtained by dividing the measured tensile force by the cross-sectional area of the sample.

The schematic depiction of the tensometer is presented in Fig. 1. The prismatic rectangular beam (10 mm-width and 40 mm-height) was clamped horizontally on the beam holder, which was assembled on the stainless steel base-stand. The cantilever beam used in this study was made of stainless steel with a Young's modulus of 193 GPa; however, different beam materials may be selected to obtain different beam compliance. A LVDT (Model: 050-HR-000; Component Distributors Inc., Ft. Lauderdale, FL, USA) was installed at the free end of the cantilever beam to record the displacement of the cantilever beam.

One unique feature of this device is the novel design of the sample assembly that facilitates convenient sample injection, experimental reproducibility, and a short preparation time between consecutive measurements. The sample assembly, as illustrated in the enlarged area

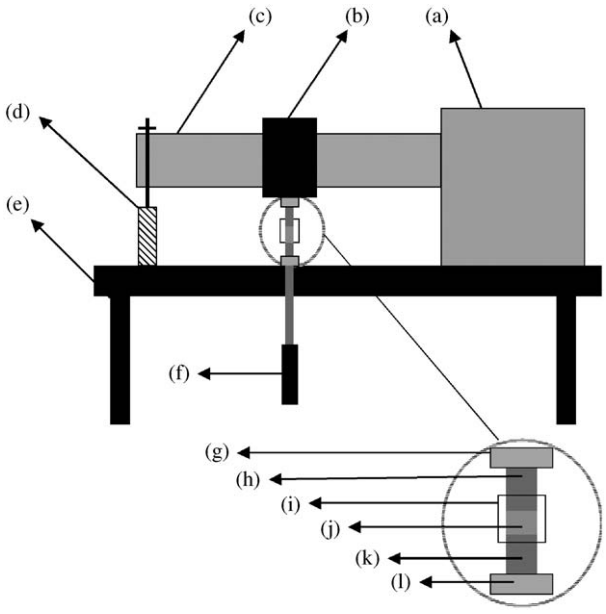

Figure 1 The ADAF shrinkage stress measurement device (data acquisition and processing control box not shown): (a) cantilever beam holder; (b) upper collet holder; (c) cantilever beam; (d) LVDT; (e) base stand; (f) curing light guide; (g) upper collet; (h) top quartz rod; (i) PTFE sleeve; (j) sample; (k) bottom quartz rod; (l) lower collet.

in Fig. 1, includes the upper collet that holds the top quartz rod, sample (bonded to the top and bottom rod), and lower collet that holds the bottom quartz rod. Before each measurement, two pieces of quartz rod were prepared and the ends were flattened and polished with 600 grit wet silicon carbide paper. One end of each quartz rod was then silanized with silane agent (Fusion bonding system, George Taub Products and Fusion Co., Inc, Jersey City, NJ, USA). The silane agent was applied on the rod end multiple times and air-dried. Once the desired upper collet holder position was chosen and secured, the top quartz rod with the silanized end pointing down was mounted into the upper collet. The bottom quartz rod was then mounted into the lower collet and aligned vertically with the top quartz rod, with the silanized end pointing up. The bottom quartz rod was employed not only to bond the sample with the sample assembly and the tensometer, but also to guide irradiation from the curing lamp to the sample. This effect was achieved by an adapter that facilitates the alignment of the light tip of the curing lamp directly underneath the lower end of the bottom quartz rod.

A polytetrafluoroethylene (PTFE) sleeve of 10 mm in length was used as sample holder and placed around the gap between the top and bottom quartz rods. The inside diameter, wall thickness, and outside diameter of the PTFE sleeve are 0.635 mm, 1.588 mm, and 9.525 mm, respectively. Two holes were drilled on two opposite sides of the PTFE sleeve beforehand: one hole of 1.5 mm in diameter for the injection of the composite sample; the other hole of 0.5 mm in diameter for the venting of air bubbles during injection. The sample height was determined with a height gauge to adjust the gap distance between the top and bottom quartz rods. Once the rods were fixed to the desired sample height, sample was injected into the sample holder to fill the gap between the silanized ends of the two rods and the horizontal boundary imposed by the PTFE sleeve. Different sample heights are readily achieved by using different height gauges to adjust the distance between the top and bottom rods, while different sample diameters are obtained by using different quartz rod diameters. Corresponding sizes of collets and sample holder sleeves need to be selected to fit with the quartz rod used. In this study, a quartz rod of 6 mm diameter was used for all experiments, and the sample height was 2.5 mm unless otherwise specified. Therefore, the sample geometry is a disk 6 mm in diameter and 2.5 mm in height, which corresponds to an aspect ratio of 2.4.

2.2. Tensometer calibration

Before any shrinkage stress measurement was made, the tensometer was calibrated to determine the beam constant at a particular collet position along the beam. The calibration was conducted by applying an incremental downward tensile load (from 0 N to approximately 100 N) on the cantilever beam and recording the corresponding LVDT readings at each load. Compressed air connected to the load calibration cylinder (Speedaire®, pressure range 0 kPa to 690 kPa (= 100 psi), Dayton Electric Mfg Inc., Niles, IL, USA) was employed as the load source. A miniature low profile universal load cell (Model: LC703-50, Omega Engineering, Inc., Stamford, CT, USA) was placed between the upper and lower collets to record the accurate tensile load value. The step size of the incremental load was approximately 10 N resulting in a table of the 10 tensile load values and the corresponding LVDT readings at each load. If a plot of the LVDT displacement reading as a function of the tensile load was not fit to a linear regression with an $R^2 \geq 0.999$, the calibration process was repeated.

2.3. Evaluation of tensometer using cantilever beam theory

To analyze and evaluate this shrinkage stress measurement device, the classical cantilever beam theory was employed. For a rectangular prismatic cantilever beam under a concentrated normal load F, the displacement at the free end of the cantilever beam caused by the load F is described using the following equation [22]. It should be noted that this equation is only valid for beam of a linearly elastic material with a small deflection.

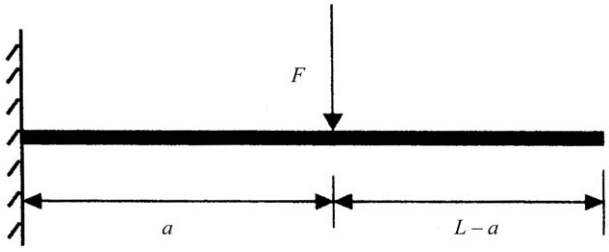

$$\frac{\varepsilon}{F} = \frac{2}{E \cdot b \cdot d^3} \cdot a^2 \cdot (3L - a)$$

in which ε is displacement at the beam end (μm); E is the Young's modulus of the cantilever beam (MPa); F is the load necessary to generate the displacement ε (N); L is the overall beam length (cm); a is the distance from the load applied position to the beginning of beam (cm); b is the beam width (cm); d is the beam height (cm).

2.4. Materials

The quartz rod was purchased from Chemglass Inc. (Vineland, NJ, USA). A light-cured hybrid dental restorative composite (TPH: lot # 021120, shade A2, Dentsply-Caulk Inc., Milford, DE, USA) was used for this study. All experiments were carried out at room temperature (23 °C ± 1 °C), and the curing light used in this study was a Spectrum® Curing Unit (Dentsply-Caulk, Milford, DE, USA). The light intensity, measured by a Demetron Model 100 radiometer (Demetron Research, Danbury, CT, USA), was 510 ± 25 mW/cm^2 at the upper end of the top quartz rod where the sample was bonded.

3. Results

Calibrations at seven different beam lengths from 5 to 20 cm were conducted, covering the majority of the cantilever beam length. From the calibration results, expressed as LVDT reading as a function of the applied load, it was obvious that a very strong linear relationship

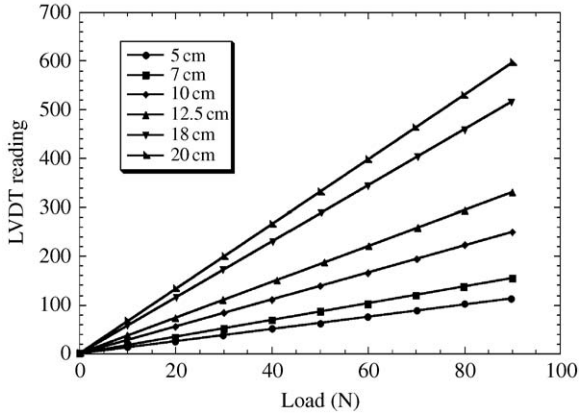

Figure 2 Calibration plot of LVDT readings vs. the applied load at different beam lengths.

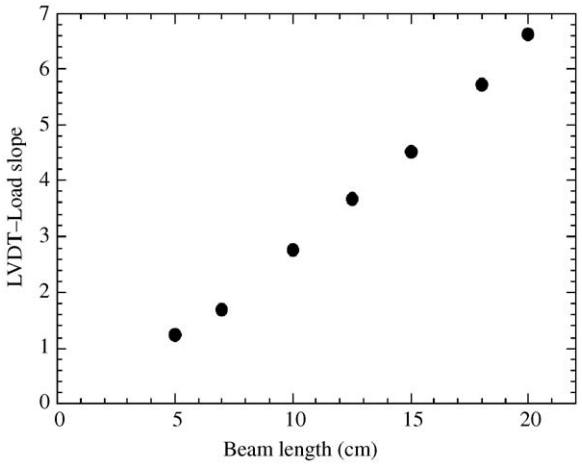

Figure 3 Slope of LVDT vs. the applied load at different beam lengths from calibration.

was obtained at each beam length ($R^2 > 0.999$) as summarized in Fig. 2. In addition, changing the beam length has a significant impact on the instrument compliance. As also shown in Fig. 2, the same applied load leads to larger beam deflection with the increase of the beam length. The slope of the deflection vs. applied load at each beam length was plotted as a function of the beam length. As demonstrated in Fig. 3, this slope increases steadily with increasing beam length, indicating the range of compliance values available for this particular beam.

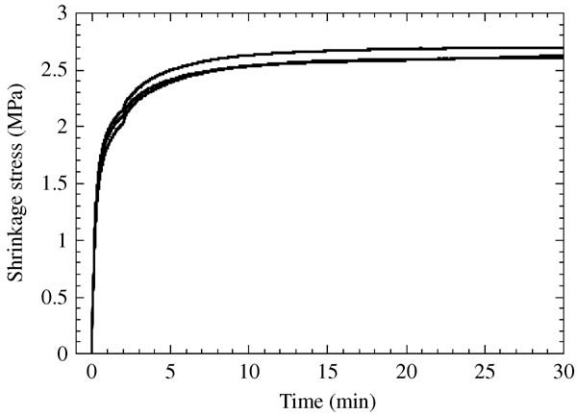

Figure 4 Shrinkage stress development of TPH at beam length of 12.5 cm ($n = 3$). The sample was cured with 510 mW cm^{-2} visible light for 120 s at $T_0 = 23\,^{\circ}$C. The standard deviation is given as the estimated standard uncertainty of the measurement.

A systematic investigation of the effect of instrument compliance on the shrinkage stress measurement was conducted. Six different beam lengths (5 cm, 7 cm, 10 cm, 12.5 cm, 15 cm, and 18 cm) were studied and compared, while keeping the curing conditions and sample dimensions constant. At each beam length, three repeated measurements were performed. As a representative set of repeated experiments, the shrinkage stress development as a function of time at the beam length of 12.5 cm is shown in Fig. 4. The same general pattern of shrinkage stress development has been observed for the stress measurements at all the beam lengths studied. The values of the shrinkage stress, tensile load, and sample displacement at 30 min after the irradiation began are presented in Table I. As the cantilever beam length increased from 5 to 18 cm, the sample displacement generated during the polymerization shrinkage rose from 0.76 to 13.88 μm, while the tensile load (shrinkage force)

TABLE I Polymerization shrinkage stress, sample displacement and load of TPH (values shown were 30 min after the irradiation began). The sample was cured with 510 mW cm^{-2} visible light for 120 s at $T_0 = 23\,^{\circ}$C ($n = 3$)

Beam length (cm)		5	7	10	12.5	15	18
Sample displacement (μm)	1	0.72	1.77	4.04	7.08	10.34	13.87
	2	0.84	1.82	4.28	7.36	10.87	13.89
	3	0.72	1.64	4.44	7.39	10.08	13.87
	Average	0.76	1.74	4.25	7.28	10.43	13.88
	SD	0.07	0.09	0.20	0.17	0.41	0.01
Tensile load (N)	1	139.10	127.62	87.72	73.76	61.04	44.82
	2	162.21	130.59	92.81	74.04	64.07	45.05
	3	137.17	117.34	95.97	76.30	59.46	44.88
	Average	146.16	125.18	92.17	74.70	61.52	44.91
	SD	13.93	6.96	4.16	1.39	2.34	0.12
Shrinkage stress (MPa)	1	4.92	4.52	3.10	2.61	2.16	1.586
	2	5.74	4.62	3.28	2.62	2.27	1.594
	3	4.85	4.15	3.40	2.70	2.10	1.588
	Average	5.17	4.43	3.26	2.64	2.18	1.589
	SD	0.49	0.25	0.15	0.05	0.08	0.004
	CV (%)	9.5	5.6	4.5	1.9	3.8	0.3

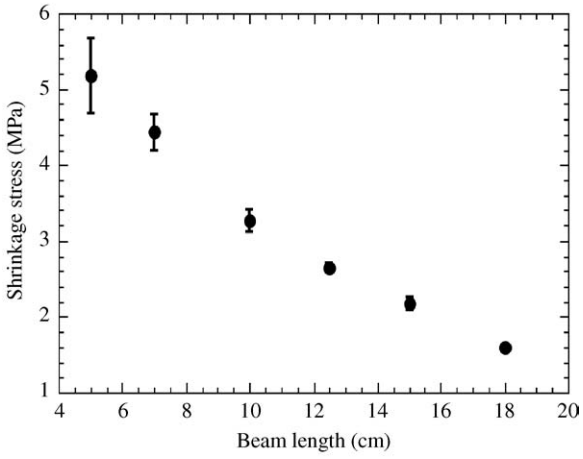

Figure 5 Shrinkage stress of composite measured at different beam length from 5 to 18 cm (values were taken at 30 min after the irradiation began). The sample was cured with 510 mW cm^{-2} visible light for 120 s at $T_0 = 23\,^{\circ}\mathrm{C}$ ($n = 3$). The standard deviation (T bars) is shown as the estimated standard uncertainty of the measurement.

applied on the tensometer decreased from 146.2 to 44.9 N. Correspondingly, the magnitudes of the shrinkage stress decreased from 5.17 to 1.59 MPa as the beam length increased from 5 to 18 cm. Fig. 5 shows the final shrinkage stress values (the stress at 30 min after the irradiation began) of the sample as the beam length changes from 5 to 18 cm. It was observed that as the measurements were performed with a longer beam length, increased reproducibility was obtained. The coefficient of variation (CV_standard deviation divided by average), as a measure of reproducibility, of the stress measurements obtained from 5 to 18 cm are also shown in Table I.

4. Discussion

As has been described in the previous section, the cantilever beam displacement at the free end of the cantilever beam was monitored using a LVDT to determine the contraction force of the shrinkage sample. Since the determination of the contraction force depends directly on the beam constant obtained from the calibration, it is therefore crucial to employ an accurate and reliable calibration technique. In addition, the calibration method should be convenient enough to be carried out at various positions along the cantilever beam. The current calibration technique using a load cell and applying the load using the pneumatic load calibration cylinder proves to be very straightforward and stable. As illustrated in Fig. 2, a very strong linear relationship can be obtained between the applied load and the corresponding LVDT readings throughout the entire cantilever range. This agrees very well with the cantilever beam bending theory: for a small deflection, the relationship between the applied normal load and the corresponding displacement should be linear [22].

One of the most important advantages of this shrinkage stress measurement device is the ability to vary the beam compliance by changing the beam length and beam materials. The cantilever beam becomes more compliant (less stiff) as the beam length increases, i.e. the sample position is closer to the free end of the cantilever beam. This result was clearly reflected in Figs. 2 and 3 in that at larger beam length, the same amount of applied load produces larger beam displacement due to the reduced beam stiffness. For the device used in this work, the cantilever beam is made out of stainless steel of Young's modulus 193 GPa. However, different beam materials, such as aluminum, can be selected to obtain different beam stiffness. The Young's modulus of the cantilever beam appears to be much higher than that of human enamel (84 GPa) and dentin (18 GPa) [23]. However, it should be kept in mind that the actual cavity geometry and type in clinical conditions are much more complicated than in the laboratory conditions, where a cylindrical disk-shaped sample configuration was exclusively used. The shrinkage stress measured assumes uni-axial tensile stress only, while the actual shrinkage stress generated is multi-axial and has a complex dependence on the cavity configuration.

The clinical implication of this compliance-controlled shrinkage stress measurement method is that every cavity-restoration complex is subject to deformation due to the inherent stiffness of tooth. This deformation is able to relieve part of the shrinkage stress generated during the polymerization of the composite. However, if the adhesion between the restorative composite and tooth were not strong enough, instantaneous adhesive failure would occur when the shrinkage stress exceeded the bond strength. Fortunately, improvements in dentin bonding agents and techniques for their application have reduced, but not eliminated, the likelihood of instantaneous adhesion failure during restoration curing [24, 25]. It is thus important to investigate the long-term competition between the interfacial shrinkage force after deformation and the cavity-restoration adhesion force. For instance, it has been reported that hygroscopic expansion of the restoration could mitigate the interfacial shrinkage stress [26].

The shrinkage stress of the composite studied at various beam length ranges from 1.6 to 5.2 MPa. The range of shrinkage stress reported here is lower than the results obtained from other researchers' experiments using the tensilometer where the sample height was maintained constant [7, 17, 27, 28]. Although the system compliance, sample configuration and testing conditions are all different, the smaller shrinkage stress values obtained using this tensilometer is primarily due to the methodological difference of the stress measurement: sample deformation was allowed to occur to accommodate a portion of the potential stress using the tensometer. In most previous experiments, the sample deformation was restricted or continuously counteracted by a feed-back displacement. Interestingly, there were a few shrinkage stress studies using a tensometer or a similar instrument where the sample deformation was not compensated for. Bowen has reported dramatically reduced shrinkage stress values when sample deformation was allowed, compared to when the sample height was kept constant [5]. Miguel *et al.* has measured the shrinkage stress of samples under controlled deformation conditions and the registered maximum stress was always below 0.8 MPa [29].

It is observed in Fig. 4 and Table I that with the increase of the beam length, the reproducibility of the

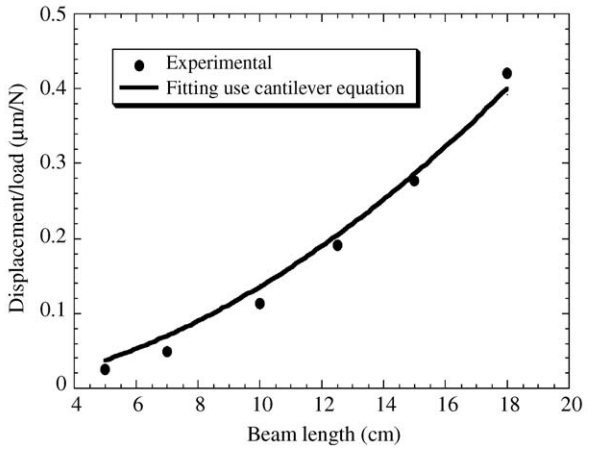

Figure 6 Experimental displacement divided by load as a function of beam length and theoretical fitting using cantilever equation.

shrinkage stress measurement was significantly improved. When the shrinkage stress was measured at 5 cm, the coefficient of variation is around 9%. At beam lengths from 10 to 18 cm, the coefficient of variation is well below 5%, and a coefficient of variation of only 0.26% was observed at beam length of 18 cm. The major reason for the reproducibility variation is that when the measurement was performed with shorter beam lengths, smaller displacements were generated by the shrinking sample. Therefore, larger measurement variation tends to arise when the beam deflection is approaching the intrinsic resolution of the monitoring device. There are several methods to overcome this limitation: first, shrinkage stress can be measured at larger beam lengths where the reproducibility is greatly enhanced. This method may be especially useful for the case where different materials or curing protocols are being compared. Second, increased numbers of replicates would be appropriate for the measurements at shorter beam lengths.

The experimentally obtained beam end displacement divided by the corresponding load was plotted versus beam length, and the result is shown in Fig. 6. The theoretical fitting of the experimental results using the above cantilever beam equation was also presented in the same figure. The theoretical curve fits the experimental data fairly well. However, there is a discrepancy of beam Young's modulus between the known value (193 GPa) and the calculated value from the fitting curve for the experimental results (143.3 GPa). The 26% variance in Young's modulus is attributed to the difference between the configuration of the actual beam and an ideal beam. The base and beam support can never be constructed to be infinitely stiff, and these assemblies will have an inherent unknown modulus of their own. Since the displacement measurement is made between the base and the beam, the actual displacement is proportional to both moduli. This is why it is imperative to have a calibration method that can determine an actual compliance constant each time the collet position is moved.

5. Conclusions

In summary, this method of determining shrinkage stress has proven to be accurate, reproducible, and practical. Instrument compliance is conveniently variable by changing the cantilever beam length. The measurement methodology based on the cantilever beam not only generates stress values but also provides sample displacement information during polymerization, which enables shrinkage stress studies to be further related to clinical restorations. The data acquisition system and the compactness of the instrument enable its facile application in the investigation of shrinkage stress kinetics of both commercial and experimental composites, as well as probing various aspects that dictate shrinkage stress development.

Acknowledgment

We want to gratefully acknowledge Brian Dickens, Ed Parry, and Tony Giuseppetti of the PRC of the ADAF for the contribution to the design and fabrication of the tensometer and software. The authors would like to thank the NIH and Department of Education for support of this research through grant #DE10959 and HL through a GAANN fellowship. We also thank Caulk-Dentsply for the donation of the composite materials.

References

1. R. M. CARVALHO, J. C. PEREIRA, M. YOSHIYAMA and D. H. PASHLEY, *Oper. Dent.* **21** (1996) 17.
2. C. L. DAVIDSON and A. J. FEILZER, *J. Dent.* **25** (1997) 435.
3. A. A. SULIMAN, D. B. BOYER and R. S. LAKES, *Dent. Mater.* **9** (1993) 6.
4. A. A. SULIMAN, D. B. BOYER and R. S. LAKES, *J. Dent. Res.* **72** (1993) 1532.
5. R. L. BOWEN, *J. Am. Dent. Assoc.* **74** (1967) 439.
6. E. ASMUSSEN, *Acta Odontol. Scand.* **33** (1975) 337.
7. A. J. FEILZER, A. J. DEGEE and C. L. DAVIDSON, *J. Dent. Res.* **66** (1987) 1636.
8. S. UNO and H. SHIMOKOBE, *Dent. Mater. J.* **13** (1994) 19.
9. Y. KINOMOTOA and M. TORIIA, *J. Dent.* **26** (1998) 165.
10. J. R. JEDRYCHOWSKI, R. G. BLEIER and A. A. CAPUTO, *J. Dent. Child.* **65** (1998) 111.
11. H. Y. CHEN, J. MANHART, R. HICKEL and K. H. KUNZELMANN, *Dent. Mater.* **17** (2001) 253.
12. T. R. KATONA and M. M. WINKLER, *J. Dent. Res.* **73** (1994) 1470.
13. G. A. LAUGHLIN, J. L. WILLIAMS and J. D. EICK, *J. Biomed. Mater. Res.* **63** (2002) 671.
14. R. L. BOWEN, K. NEMOTO and J. E. RAPSON, *J. Am. Dent. Assoc.* **106** (1983) 475.
15. C. L. DAVIDSON, A. J. DE GEE and A. J. FEILZER, *J. Dent. Res.* **63** (1984) 1396.
16. R. BRAGA and J. FERRACANE, *ibid.* **81** (2002) 114.
17. M. R. BOUSCHLICHER, F. A. RUEGGEBERG and D. B. BOYER, *J. Esthet. Dent.* **12** (2000) 23.
18. Y. TANI, T. NAMBU, A. ISHIKAWA and S. KATSUYAMA, *Dent. Mater. J.* **12** (1993) 182.
19. A. A. SULIMAN, D. B. BOYER and R. S. LAKES, *J. Prosthet. Dent.* **71** (1994) 7.
20. G. J. PEARSON and S. M. HEGARTY, *Biomaterials* **8** (1987) 473.
21. D. C. WATTS, A. S. MAROUF and A. M. AL-HINDI, *Dent. Mater.* **19** (2003) 1.
22. J. M. GERE, in ''Mechanics of Materials'' 5th edn (Brooks/Cole, Pacific Grove, CA, 2001).
23. W. J. O'BRIEN, ''Dental Materials and Their Selection'' 2nd edn (Quintessence Publishing Co Inc, Chicago, IL, 1997).
24. N. NAKABAYASHI, *Biomaterials* **24** (2003) 2437.
25. J. D. EICK, A. J. GWINNETT, D. H. PASHLEY and S. J. ROBINSON, *Crit. Rev. Oral Biol. Med.* **8** (1997) 306.

26. A. J. FEILZER, A. J. DEGEE and C. L. DAVIDSON, *J. Dent. Res.* **69** (1990) 36.
27. A. J. FEILZER, A. J. DEGEE and C. L. DAVIDSON, *Dent. Mater.* **9** (1993) 2.
28. J. R. CONDON and J. L. FERRACANE, *J. Dent. Res.* **77** (1998) 59.
29. A. MIGUEL and J. C. DE LA MACORRA, *Dent. Mater.* **17** (2001) 241.

Received 6 February
and accepted 8 April 2004